CHEMPHYSCHEM

DOI: 10.1002/cphc.200900615

From Branched Networks of Actin Filaments to Bundles

Yifat Brill-Karniely,[a] Yaron Ideses,[b] Anne Bernheim-Groswasser,[b] and Avinoam Ben-Shaul*[a]

Dedicated to Professor Erich Sackmann on the occasion of his 75th birthday

Cross-linking proteins can mediate the emergence of rigid bundles from a dense branched network of actin filaments. To enable their binding, the filaments must first bend towards each other. We derive an explicit criterion for the onset of bundling, in terms of the initial length of filaments *L*, their spacing *b*, and cross-linker concentration *f*, reflecting the balance between bending and binding energies. Our model system contains actin, the branching complex Arp2/3 and the bundling protein fascin. In the first distinct stage, during which only actin and Arp2/3 are active, an entangled aster-like mesh of actin filaments is formed. Tens of seconds later, when filaments at the aster periphery are long and barely branched, a sharp transition takes place into a star-like structure, marking the onset of bundling. Now fascin and actin govern bundle growth; Arp2/3 plays no role. Using kinetic Monte Carlo simulations we calculate the temporal evolution of *b* and *L*, and predict the onset of bundling as a function of *f*. Our predictions are in good qualitative agreement with several new experiments that are reported herein and demonstrate how *f* controls the aster-star transition and bundle length. We also present two models for aster growth corresponding to different experimental realizations. The first treats filament and bundle association as an irreversible sequence of elongation–association steps. The second, applicable for low *f*, treats bundling as a reversible self-assembly process, where the optimal bundle size is dictated by the balance between surface and bending energies. Finally, we discuss the relevance of our conclusions for the lamellipodium to filopodia transition in living cells, noting that bundles are more likely nucleated by "tip complex" cross-linkers (e.g. mDia2 or Ena/VASP), whereas fascin is mainly involved in bundle maintenance.

1. Introduction

Cell locomotion is essential for many vital biological processes, such as the development of tissue patterns in embryogenesis, or fibroblast migration in wound healing. Unfortunately, it also plays a detrimental role in the formation of cancerous metastases. Cell movement is driven by the dynamic growth of polar actin networks of various structures,[1–6] e.g. the lamellipodium—a broad (~10 μm) and thin (~0.2 μm) compartment containing a dense gel of branched "living" actin filaments.[1,7] Actually, it was demonstrated that even a fragment of the cell containing the lamellipodium, but lacking the nucleus, microtubules and other organels can perform movement on its own.[8]

The F-actin filaments are polar, elongating and branching towards the cell's leading edge by adding actin monomers (G-actin) to their barbed (or "plus") ends. Depolymerization takes place at the other, pointed ("minus") ends, performing a treadmilling dynamics whereby the actin gel grows in the direction of movement and retracts at the rear.[1,9,10] The actin network of moving cells is tightly linked to the substrate via dynamical adhesion complexes,[11–14] enambling the growing actin network to push against the cell membrane,[1,15] providing the driving force for protrusion and cell movement.[16] In some cells, such as keratocytes for example, lamellipodium is the only protrusion observed.[1,2] On the other hand, many other cells (e.g. nerve growth cones, several amoeba, many cancer cells) show thin protrusions that emanate from the lamellipodia surface.[2,17,18] Commonly found structures are the filopodia. These finger-like extensions are composed of bundles of parallel actin filaments that protrude into and push forward the plasma membrane. The filopodia enhance cell adhesion to the extra-cellular substrate[19] and function in the sensing cell environment.[20] They may also enhance the invasiveness of cancer cells.[20–22]

The dynamical emergence of filopodia from the branched actin network of the lamellipodia has been extensively studied. Two possible mechanisms have recently been proposed. According to the first model, filaments in the surface of the branched network elongate and cross-link with each other to form bundles, which gradually increase in both thickness and length, resulting in the appearance of stable filopodia.[23–25] The second model proposes that filopodia are formed following an independent nucleation, assembly and growth of filaments that are not anchored to the lamellipodia.[17,26,27] Herein, we an-

[a] *Y. Brill-Karniely, Prof. A. Ben-Shaul*
Institute of Chemistry and Fritz Haber Center
Hebrew University, Jerusalem 91904 (Israel)
Fax: (+972) 2-6513742
E-mail: abs@fh.huji.ac.il

[b] *Y. Ideses, Dr. A. Bernheim-Groswasser*
Department of Chemical Engineering
Ben-Gurion University of the Negev
Beer-Sheva 84105 (Israel)

Supporting information for this article is available on the WWW under http://dx.doi.org/10.1002/cphc.200900615.

alyze theoretically a series of in vitro experiments, partly described here and in more detail elsewhere,[28,29] which appear to support the first mechanism. More explicitly, in the next section we show, both experimentally and theoretically, that in the presence of fascin, a dense and highly branched aster-like network of actin filaments exhibit a transition to a star-like structure, where bundles of filaments emanate and grow radially from the aster-like core.

Our in vitro system contains actin, the cross-linking protein fascin, the branching complex Arp2/3 and the constitutively active VCA (or WA) domain of WASp, which activates the Arp2/3 complex.[30,31] Previous work showed that upon mixing these components Arp2/3 plays a dominant role in the early stages of actin network formation, resulting in the appearance of densely branched, nearly spherical, aster-like structures.[28,29] Fascin comes into play at a later stage, when the filaments at the aster surface are long and sparsely branched. Now the filaments can bend toward each other, enabling fascin to cross-link them into finger-like bundles, resulting in a structural transition from a dense aster to a large star-like structure.[28,29] The similarity between the aster-to-star and the lamellipodium-to-filopodia transitions underlies our in vitro experimental studies and their theoretical interpretations.

In previous studies we presented simulations and theoretical models describing the formation of the branched asters,[28] and briefly considered their transition to stars.[29] Other authors[32] examined the formation of stars, assuming that the filaments are randomly located and oriented within the aster, without taking into account the branched structure of the aster. Recently, we have studied experimentally the competing roles of Arp2/3 and fascin in the aster-to-star transition, and a stepwise "elongation–association" mechanism of bundle growth has been proposed.[29] The present study is mostly theoretical, focusing on the role of fascin in determining the onset of bundle formation, as well as in the subsequent elongation and thickening of the bundles. Several new experiments along these lines are also presented here.

One of our major goals herein is to explain, theoretically, the importance of filament length in the bundling process, as has recently been observed both in vivo[24,25,33–35] and in vitro.[29,36,37] The basic theoretical premise underlying our theoretical analysis is that bundle formation sets in when neighboring filaments emerging from the surface of the aster get long enough, to enable them to bend towards each other and cross-link (e.g. with fascin) to nucleate a stable dimer. The dimer can subsequently associate with other filaments to form larger bundles. The binding energy should of course exceed the bending energy penalty. In Section 2.1 we present a simple model which casts this notion in more quantitative terms, taking into account the structural characteristics of the actin-aster periphery, and a fascin-dependent geometrical criterion for bundling is derived. A simple interplay between two length scales determines the onset of bundling: the average distance, b, between the origins (i.e. pointed ends) of neighboring filaments and their length, L. In Section 2.2 we use kinetic Monte Carlo (KMC) simulations to derive these quantities as a function of time, and delineate the aster-to-star transition as a function of fascin concentration, f. We then describe two models for bundle growth in Section 2.3. The first assumes a kinetically controlled, step-wise irreversible elongation–association mechanism applicable at high fascin concentrations. This model has been described previously and is sketchily outlined herein, mainly for the sake of comparison. The second model treats the association of actin filaments as a reversible process, governed by equilibrium consideration. This "equilibrium self-assembly" model is relevant for low fascin concentrations, when filament association and dissociation are faster than their elongation.

In Section 3, apart from summarizing our findings, we critically discuss the various assumptions employed in our models, as well as their relevance to the lamellipodium-to-filopdia transition in living cells. In particular, it will be stressed there that the nucleation of bundles in living cells is actually mediated by other cross-linking proteins, such as mDia2 formin and Ena/VASP, whereas fascin is mainly relevant for the subsequent stabilization and growth of the bundles.[34] Yet as in our in vitro experiments, where fascin is the sole cross-linker, the initial filament length, and hence its bending energy, is the major factor determining the onset of bundling.

2. Results and Discussion

2.1. F-actin Dimerization

The actin filaments in the interior of the aster are highly branched, entangled and densely packed.[28] They are also very rigid (persistence length of $\xi \sim 10$ μm[38,39]), and within the aster core cannot even bend slightly, owing to strong excluded-volume interactions. Thus, bundle formation can only take place at the aster's periphery where, on average, the filaments are relatively long, barely branched, and not entangled with each other.[28,29]

The association of two neighboring filaments into a dimer (Figure 1) can be regarded as, and most likely is, the first step in bundle nucleation. The free energy change per filament in this process, given by Equation (1):

$$\Delta F_2 = E_{\mathrm{bend}} + \Delta F_{\mathrm{bind}} \qquad (1)$$

is the sum of the (unfavorable, $E_{\mathrm{bend}} > 0$) bending energy, and the cohesive binding energy ($\Delta F_{\mathrm{bind}} < 0$). Here, we ignore other, much smaller, contributions to ΔF_2, such as the loss of orientational entropy of the filaments.[40] To calculate the two

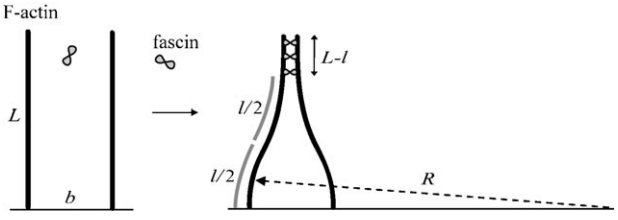

Figure 1. Schematic illustration of dimer formation by two neighboring filaments of initial length L, whose origins are a distance b apart. The bent portions of the filaments, of length l each, are modeled as composed of two smoothly connected identical arcs (gray). R is their radius of curvature.

free energy terms we assume, as in Figure 1, that once a dimer is formed from two filaments of total length L, it consists of a bent part (the "root") where filament length is l, and a straight "stem" of length $L–L$ where the two filaments are cross-linked and run parallel. At their other (pointed) ends the filament roots are perpendicular to the surface. Since L and b are much smaller than the radius of the aster, its surface may safely be treated as being planar.[29] Assuming that all filaments are initially normal to the surface is a simplifying assumption.[29,40]

Both b and L are small compared to ξ, hence the curvatures of the bent parts (l in length) are very small. We approximate their geometry as composed of two smoothly connected arcs, as illustrated in Figure 1, (similar to a previous geometry that has been calculated rigorously[40]). Simple geometric considerations then lead to $R \sim l^2/4b$ for the radius of curvature of the (four) curved arcs. The bending energy, per arc, is thus $\kappa(l/2)/R^2 = 8\kappa b^2/l^3$ where $\kappa = (1/2)\xi kT$ is the bending modulus of the filament. The bending energy of a filament caused by dimer formation is thus given by Equation (2):

$$E_{bend} = \chi b^2/l^3 \qquad (2)$$

with $\chi \equiv 8\xi kT$.

The dimer binding free energy (per filament) is proportional to the length of the stem, $\Delta F_{bind} = (L-l)\Delta E_{fas}$ with ΔE_{fas} denoting the binding energy per unit length. To calculate ΔE_{fas} we note that fascin can bind to an actin dimer in one of two ways, as illustrated in Figure 2a by simultaneously binding to two properly apposed sites, thus cross-linking the two filaments, or to only one of the filaments. Owing to the helical arrangement of binding sites around the F-actin axis,[41,42] when two filaments are aligned parallel to each other, only 1/6 of the sites can be populated by doubly bound cross-linker fascin, the other (5/6 of the total) binding sites of the dimer can potentially bind a fascin protein via one of its two ends—making no contribution to filament dimerization. Thus, on a filament dimer, within a length equal to the F-actin helix period ($\lambda \approx 0.072$ μm[41]) there are ten "singly bonding" sites (hereafter S-sites) and one "doubly bonding" site (hereafter D-site). On a single filament there are of course six S-sites per helical turn, and no D-sites. The actual occupation probabilities of the S- and D-sites by fascin depend on the concentration, f, of free linker in solution and the binding energies corresponding to the two sites. The change per filament unit length, in the fascin-mediated binding energy when two isolated filaments join into a dimer is $\Delta E_{fas} = (10\theta_S\varepsilon_S + \theta_D\varepsilon_D - 12\theta_S\varepsilon_S)/2\lambda$, where θ_S and θ_D are the occupation probabilities of the S- and D-sites, respectively. Following previous studies[43] we use $\varepsilon_S = -10kT$ and assume that $\varepsilon_D = 2\varepsilon_S = -20kT$.

The occupation probabilities are dictated by the requirement of chemical equilibrium between free and bound fascin molecules. That is, the chemical potentials of free, singly-bound, and doubly-bound fascin must all be equal: $\mu_S = \mu_D = \mu_f$ where μ_f, μ_S, μ_D are, respectively, the chemical potentials of free in solution, singly bound, and doubly bound fascin. The actin filaments, in both the monomeric and dimeric states, can be adequately treated as 1D lattices of binding sites, with 10 S-sites and one D-site per helix turn in the dimer, and 6 S-sites per turn in the monomer. This implies the familiar expressions $\mu_D = \varepsilon_D + kT\ln[\theta_D/(1-\theta_D)]$ and $\mu_S = \varepsilon_S + kT\ln[\theta_S/(1-\theta_S)]$. For the free fascin in solution we can safely assume dilute solution behavior, and hence $\mu_f = kT\ln(f/f_0)$ where f_0 is a reference ("standard") molar concentration, whose numerical value ($f_0 = 2.72\times107$ μM) was determined based on experiment, as explained in the Supporting Information. From the equilibrium conditions $\mu_S = \mu_f$ and $\mu_D = \mu_f$ we now obtain the Langmuir-like adsorption isotherms, shown in Equation (3):

$$\theta_i = \frac{K_i f}{1 + K_i f} \quad (i = S,D) \qquad (3)$$

with $K_i \equiv (1/f_0)\exp(\varepsilon_i/kT)$. For the binding energy per unit length we get Equation (4a):

$$\Delta E_{fas} = \frac{\varepsilon_S}{\lambda}\left(\frac{K_D f}{1 + K_D f} - \frac{K_S f}{1 + K_S f}\right) \qquad (4a)$$

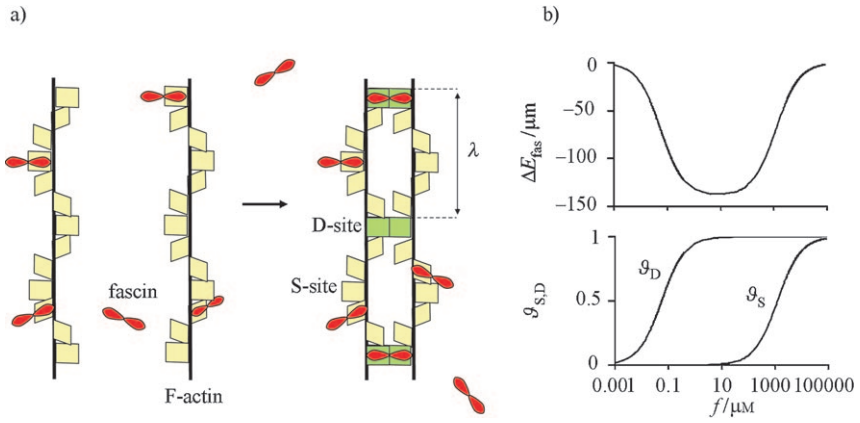

Figure 2. A structural model for calculating the fascin-mediated dimerization of two actin filaments. a) The fascin binding sites are arranged helically around the axis of F-actin, λ denoting the helix period. In the monomeric F-actin there are 6 fascin binding sites per helical turn. In the dimer two of the 12 sites align to form one "double" (D-) site which can only be occupied by a doubly connected, dimer linking, fascin. The other 10 sites are no different from the S-sites of monomeric F-actin. b) The occupation probabilities, θ_S and θ_D of the D- and S-sites, respecively, as a function of fascin concentration in solution, f, (bottom panel). Also shown is the f dependence of dimer formation energy (top panel).

Using $\varepsilon_D = 2\varepsilon_S = -20kT$ we have calculated the binding probabilities θ_i and ΔE_{fas}as a function of f: the results are shown in Figure 2b. In the few in vitro experiments reported herein and those described in more detail elsewhere,[28,29] the relevant fascin concentrations are much lower than 10 μM. In this regime $\theta_i \ll \theta_D$, reflecting the stronger energetic prefer-

ence of the fascin to populate the D-sites (Figure 2b). This trend persists and ΔE_{fas} consequently decreases (i.e. stronger binding) as f increases, until it reaches an intermediate value, $f \approx 10$ μm in our case. Above this concentration, all the D-sites are already saturated, and fascin from solution begins populating the non-bonding S-sites. θ_S continues to increase with f all the way to saturation ($\theta_S \to 1$). In this high-f regime, fascin from solution saturates the S-sites of the monomeric F-actin as well, and the drive for filament dimerization gradually decreases and eventually vanishes ($\Delta E_{fas} \to 0$). [There is a small entropic gain associated with the release to solution of one fascin molecule whenever two initially populated S-sites of monomeric actin are replaced by a doubly connected D-site; but its value is negligibly small, especially when f is large. We ignore this entropic gain here.] Previously, the cross-linking energy was calculated assuming $\theta_S = 0$ and $\theta_D = 1$.[29] Here we are specifically interested in the low-f regime ($f \leq 10$ μm), where $\theta_D \leq 1$. Note, however, that in this regime $\theta_S \approx 0$, and instead of Equation (4a) we simply have Equation (4b):

$$\Delta E_{fas} = \frac{\varepsilon_S}{\lambda} \frac{K_D f}{1 + K_D f} \tag{4b}$$

Using Equations (1) and (2) we obtain Equation (5):

$$\Delta F_2 = \chi b^2 / l^3 + (L - l)\Delta E_{fas} = \chi b^2 / l^3 + (L - l)\varepsilon_S K_D f / \lambda (1 + K_D f). \tag{5}$$

The necessary condition for the formation of a stable dimer is $\Delta F_2 < 0$. For given L, b and f, this condition may be fulfilled by a range of l values. The optimal l is found by minimizing ΔF_2, yielding $l^* = (-3\chi/\Delta E_{fas})^{1/4} b^{1/2}$. We can now express ΔF_2 as a function of the two geometrical parameters L and b, [Eq. (6)]:

$$\Delta F_2 = \Delta E_{fas} L + 1.75 \chi^{1/4} (-\Delta E_{fas})^{3/4} b^{1/2} \tag{6}$$

and the necessary condition for dimer formation ($\Delta F_2 < 0$) is given by Equation (7) as an inequality:

$$b < (|\Delta E_{fas}|/9.4\chi)^{1/2} L^2 \tag{7}$$

Since dimer formation is the first step for filament bundling we interpret this last inequality as the geometrical condition defining the onset of actin bundling.

2.2. Modeling the Onset of Bundling: Aster-to-Star Transition

The first stage in the in vitro experiments of actin polymerization in the presence of Arp2/3 and fascin is the nucleation and growth of aster-like networks. Fascin molecules play no role in this process owing to the high density and frequent branching of the filaments within the aster core.[28,29] Arp2/3 continues binding and nucleating branches everywhere in the aster, including from the older filaments in the interior of the aster. The density and degree of branching falls rather sharply at the aster's periphery.[28,29] Therefore, only the sparsely branched filaments emanating from the outermost layer of the aster can possibly bend toward each other and start associating into bundles with the aid of fascin. In our experiments this happens when the concentration of G-actin begins to fall off due to its consumption in the course of aster growth, as we show below. According to a detailed kinetic analysis,[44] branch nucleation is a third-order rate process, requiring two G-actin molecules and one Arp2/3 complex, whereas actin polymerization is a pseudo-first-order process. Thus the rate of branching falls off more rapidly with time than the rate of polymerization, and the radially expanding[28] surface of the aster consequently consists of relatively long and barely branched filaments. These are the filaments which nucleate bundling. Once bundles begin to grow in length and thickness, branching becomes even less likely, mainly because it cannot take place inside the tightly bound bundle.

Consistent with this qualitative picture, our experiments show that stars begin to appear only after a time lag, t_{tr}, of a few minutes after mixing all components in solution. Arp2/3 dominates the first stage of aster growth and maturation, becoming irrelevant in the second, star-formation, stage when fascin is the dominant factor.[28,29] All the actin left at t_{tr} becomes available for the formation of bundles.

In Section 2.3, we describe two theoretical models, corresponding to different experimental realizations. Our basic assumption in both cases is that inequality of Equation (7) must be fulfilled, marking the onset of bundling. To this end we need the time dependence of L and b, which cannot be measured experimentally but can be calculated using our KMC simulations. In previous studies we have shown that these simulations account adequately for experimental observations.[28,29] The simulations allow for filament growth and branching (as well as capping and possibly severing), but do not account for filament bending, which requires different computational tools. For this reason we use theoretical models to describe the bundling, using the KMC simulations to provide the input parameters of the models, L and b.

Figure 3 shows a snapshot of an aster modeled using the KMC simulation. At $t = 0$ there were 4.6×10^7 G-actin monomers and 1.5×10^6 Arp2/3 molecules in the simulation box, corresponding to initial concentrations of [G-Actin] = 3 μM and [Arp2/3] = 100 nM. Polymerization and branching processes are taken into account and their rates are calculated using known rate constants, with the concentrations varying in time accordingly.[28] The transformation from Monte Carlo steps to real time is a standard procedure, as described earlier.[28] The value of L is determined as the length of a peripheral, unperturbed, filament. (For concreteness we allow, on average, for one branch along L, between the pointed end where the filament is anchored to its mother filament and its tip.) For b we take the average distance between the (fixed) origins of neighboring filaments. The calculations provide many additional quantities; of relevance here are the total number, M, of filaments emanating from the surface of the aster and the concentrations of free and bound proteins.

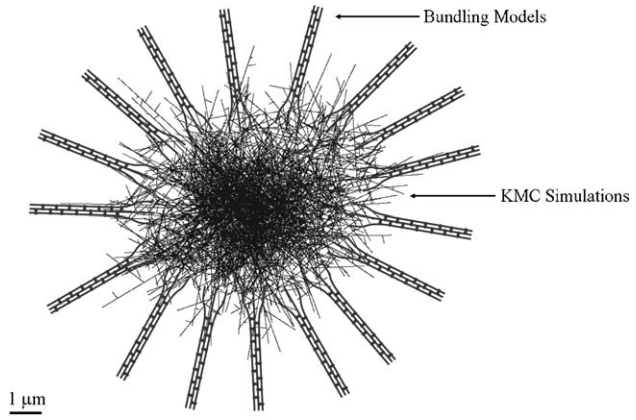

Figure 3. Structural model for the aster-to-star transition. The dense, radially symmetric and highly branched actin network nucleates from a single seed at the center of the aster-like core. When the filaments at the surface of the aster are long enough they can bend towards each other and with the help of fascin, bundles begin to form, signaling the onset of the star-like aggregate. The structure of the aster is calculated using kinetic Monte Carlo simulations; the straight narrow lines represent the branched network of actin filaments. Star formation is then modeled using several bundling theories.

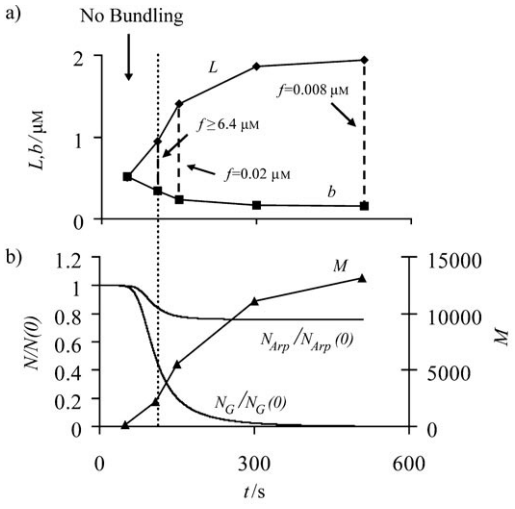

Figure 4. a) Time-dependence of L and b as predicted by a KMC simulation of aster growth, with initial actin and Arp2/3 concentrations corresponding to 3 μM and 100 nM, respectively. The dashed vertical lines mark the pairs of L and b corresponding to the dimensions of the "critical aster", marking the onset of the transition to a star, for the given values of f. b) KMC simulations results showing the change in time of the total numbers, N_G and N_{Arp}, of free G-actin and Arp2/3 molecules in the system, respectively, divided by their values at $t=0$. (left ordinate). Also shown is the change in time of the number, M, of filaments emanating from the surface of the aster and are available for bundling (right ordinate). The dotted line corresponds to the earliest time ($t=108$ s) at which L and b satisfy the inequality given by Equation (7), making bundling possible.

The filament binding energy ΔE_{fas} is strongest, reaching a minimum, ΔE^*_{fas}, at a certain linker concentration, f^*. In our case $\Delta E^*_{fas} = -137\,kT$ and $f^* \approx 10$ μM , (see Figure 2b). For these values, Equation (7) implies that bundling cannot occur if $L^2/b < 2.3$ μm. According to our KMC simulations, for the concentrations tested herein, the earliest time at which the aster is large enough so that $L^2/b \geq 2.3$ μm, enabling bundle nucleation, is 108 s—the age of the aster shown in Figure 3. For this aster $L = 0.94$ μm and $b = 0.34$ μm, and bundling may start, provided that $f \geq 6.4$ μM. Note that raising f above 6.4 μM will not reduce onset time.

For lower values of f and hence of ΔE_{fas} bundling sets in at higher values of the ratio L^2/b. From our KMC simulations we know that (in systems with given total concentrations of G-actin and Arp2/3) this ratio increases with time, see Figure 4a. For the three values $f = 6.4$, 0.02 and 0.008 μM presented in the figure, the predicted bundling onset times are approximately 108, 150 and 500 seconds, respectively. These findings are in good qualitative and quantitative agreement with experiments performed using similar initial concentrations of actin, fascin and Arp2/3. In these experiments star-like actin networks were first observed a few minutes after mixing the protein components in solution.

Soon after their nucleation, the bundles begin elongating and thickening. Being strongly held by the fascin cross-linkers, the filaments do not slip along each other,[45,46] and the bundles behave as rather stiff rods emanating radially from the surface of the aster outwards, gradually consuming all the available G-actin monomers left in solution. Assuming that polymerization at the growing ends is practically irreversible,[9,10] it follows that the final length of the bundled filaments is $L + N_G a/M$ where N_G is the number of actin monomers left in solution at t_{tr}. $a \approx 2.6$ nm is the length, per monomer, along the F-actin axis,[41] and M is the number of filaments available for bundling in the "critical" aster at the time of transition. The final radius of the star when practically no G-actin is left in solution, so that its structure is no longer changing, is given by $R_{star} = L + N_G a/M + R_{aster}$, where R_{aster} is the radius of the aster.

What Figure 4 actually shows are the results of KMC simulations of one aster, with initial conditions corresponding to an in vitro experimental system with the initial concentrations [G-Actin] = 3 μM and [Arp2/3] = 100 nM, and varying concentrations of fascin. Note, however, that fascin is not present in our simulations, not even implicitly. Its concentration, as explained in detail above, is used to theoretically determine the values of L, b, M and the time t_{tr} when bundling sets in. Figure 4a shows the temporal evolution of L and b, and Figure 4b shows the changes in N_G and N_{Arp}. Also shown is the time evolution of M, the number of filaments at the aster's periphery.

Part of the initial G-actin reservoir is consumed in the course of aster growth, while the remaining molecules are used in the buildup of bundles at $t > t_{tr}$. As noted above, the final length L_{fin} of the bundles, and hence R_{star} depend on N_G at t_{tr} which, in turn, depend on the fascin concentration, f. Figure 5A shows R_{star} as derived from our simulations for several selected values of f. Also shown are experimentally measured values of R_{star} for four values of the fascin concentration. Experimental snapshots of stars corresponding to the same fascin concentrations are shown in Figure 5B. Similar quantitative behavior has been demonstrated in previous experiments, where the actin concentration was 7 μM.[29]

The increase in bundle length reflects the larger reservoir of actin monomers available at the onset of the aster-to-star transition. This, in turn, depends on f, because by increasing f we

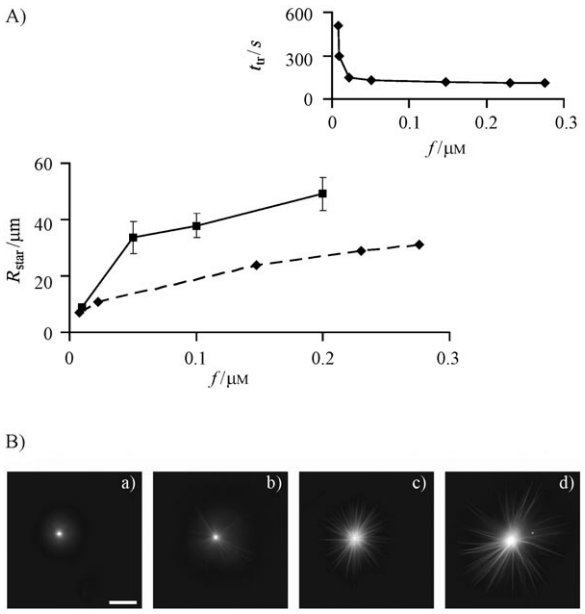

Figure 5. A) The radius of fully grown stars as a function of fascin concentration in solution, experimental (——) and theoretical (-----) results. The experimental results correspond to the four values of *f* in B, below. Inset: theoretical results showing the sharp initial decrease with *f* of the aster-to-star transition time, and the plateau at higher concentration. The plateau reflects the fact that no matter how large *f* is, the ("free") filaments at the aster's periphery must first become long enough so as to be able to bend towards each other in order to satisfy the inequality given by Equation (7). In our case this necessary condition is first fulfilled when $t \approx 108$ s; increasing *f* cannot reduce t_{tr} below this value. B) Four representative snapshots of stars in experimental systems containing initially 3 μM actin monomers (G-actin, 10% fluorescently labeled with Alexa 568), 100 nM Arp2/3 complex, 200 nM GST-VCA and four concentrations of fascin: a) 10 nM, b) 50 nM, c) 100 nM, and d) 200 nM. The medium contained 10 mM HEPES, pH 7.7, 1.7 mM Mg-ATP, 5.5 mM DTT, 0.12 mM Dabco [an anti-bleaching reagent], 0.1 M KCl, 1 mM MgCl2, 1% BSA. (bar = 20 μm).

facilitate the onset of the transition, that is, t_{tr} decreases and thus a larger number of monomers is left for bundling. For times earlier than 108 s, filaments at aster surface are short and thus the inequality of Equation (7) is not fulfilled, no matter how high *f* is (Figure 5 A, inset). Therefore, increasing *f* above a critical value (in our case −6.4 μM) does not further reduce t_{tr} and as a result R_{star} cannot increase further. We note that the experimental behavior is qualitatively well reproduced by the theoretical model for the onset of bundling. However, the experimental results for the length of the arms appear consistently larger than the theoretical ones. Several reasons could possibly explain this difference, the most likely one is that the actual actin reservoir in the experiment is larger than our estimates owing to depolymerization within the aster core, or due to fragmentation of some small and/or unstable neighboring asters in solution.

2.3. Bundle Growth and Dimensions

Bundle nucleation sets in once the fascin-mediated binding energy of two filaments overcome their bending energy. Hereafter bundles can grow in length and thickness following different possible mechanisms. In this section we outline two bundle growth mechanisms, corresponding to different experimental realizations.

2.3.1. Irreversible Elongation–Association

Following the initial association of filaments into dimers, or small oligomers, the filaments may continue elongating by polymerization at the barbed ends. Once long enough, bending fluctuations can bring the thin bundles close to each other, and in the presence of fascin they can associate into thicker bundles. Now the thicker bundles elongate, eventually becoming long enough to bend towards each other, possibly associating into even thicker bundles. This step-wise elongation–association mechanism can in principle proceed as long as actin monomers and fascin linkers are available. It should be noted, however, that the bending rigidity of the bundles increases sharply with their thickness. If the actin filaments are strongly glued together and thus cannot slip by each other, the bending rigidity (ξkT) is proportional to the fourth power of the bundle's diameter, hence to N^2, where *N* is the number of filaments in the bundle.[45–47] This, in turn, implies that the length of the elongating bundles must rapidly increase from one generation to another, as illustrated in Figure 6.

The above scenario assumes that bundle association is irreversible. This assumption is most reasonable when *f* is high, in which case many fascin molecules are present in the interior of

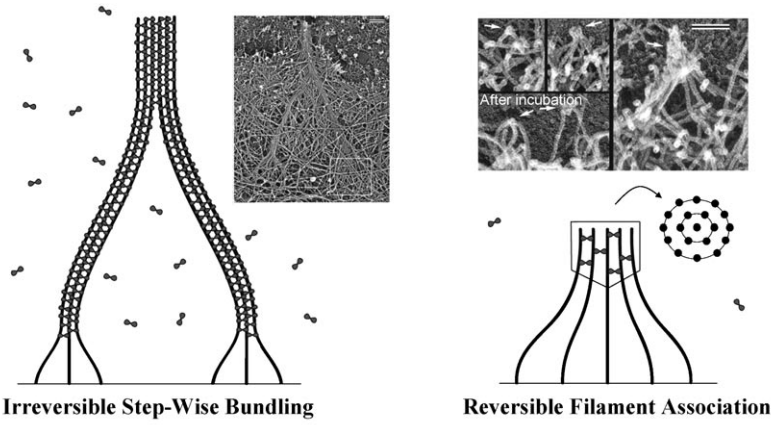

Figure 6. Two models of bundle growth. Left: Irreversible step-wise bundling, applicable to in vitro bundle growth at high *f*, reminiscent of the gradual growth of filopodia in vivo, as observed in the EM image shown. Right: Equilibrium model for reversible filament association. This model describes in vitro bundling when *f* is low, resembling bundle nucleation in living cells, as shown in the EM image. EM images: © Svitkina et al., 2003. Originally published in *J. Cell Biol.* **2003**, *160*, 409–421.[34]

bundles, each contributing about $20\,kT$ to the cohesiveness of the bundles. This step-wise behavior resembles some electron micrographs depicting the emergence of filopodia from the entangled mesh of actin filaments in the cytoskeleton of melanoma cells, Figure 6 (left). The step-wise mechanism has been described in more detail in our previous study,[24] which has focused on the interplay between Arp2/3 and fascin in determining the length and thickness of the bundles in in vitro aster-to-star transitions.

2.3.2. Equilibrium Self-Assembly of Filaments

On purely thermodynamic grounds the filaments constituting a mature bundle are essentially irreversibly associated on any relevant experimental time scale, even at moderate cross-linker concentrations. On the other hand, soon after the onset of filament dimerization, when the stems of the dimers (see Figure 1) are still short and relatively weakly held together, the dimers (as well as other thin, short actin oligomers) can reversibly dissociate and associate, self-assembling into an equilibrium distribution of bundle sizes. This scenario is, of course, only applicable when the rates of filament association–dissociation are larger than that of actin polymerization. These processes depend, in turn, on the concentrations of actin and fascin in solution. For example, in our in vitro studies of the aster-to-star transition (with initial concentrations [G-actin] = 3 μM and [Arp2/3] = 100 nM), these conditions appear appropriate for $f <$ 0.01 μM, supported by methods presented elsewhere.[25,40] Recall that when the concentrations of fascin are that low, the aster-to-star transition takes place relatively late, when the number of actin molecules left in solution is indeed small (see Figure 4 and Figure 5) and the bundles are consequently necessarily short. Furthermore, for these very low fascin concentrations only a fraction ($\theta_D < 1$) of the D-sites are occupied.

As before, the growth is controlled by the interplay between the bending energy, which disfavors bundling, versus the favorable cross-linker mediated filament adhesion. Entropy losses of filament upon bundling are small and are not taken into account. The role of the cohesive energy actually enters through the unfavorable surface energy associated with filaments at the surface of the bundles. More explicitly, suppose, hypothetically, that the filament origins were mobile, rather than anchored to the surface. Then on purely energetic grounds, the filaments would of course tend to organize into one infinitely thick bundle. Chopping this bundle into smaller ones involves breaking cross-linker bonds, resulting in additional surface area where filaments posses new S-sites instead of their former D-sites. This explains the unfavorable surface energy of a system with many thin bundles as compared to few thick ones. However, in our system the filaments are immobile and they must bend in order to approach each other, which also mean that they must be long enough to do so. The bending energy penalty obviously increases with the width of the bundle, because its constituent filaments are, on average, farther apart from each other. We thus expect that there will be some specific (average) bundle size reflecting the optimal balance between the bending surface energies.

We treat the aster surface as a planar surface decorated with M actin filaments of length L. For simplicity, their origins are assumed to be anchored to the vertices of a 2D hexagonal lattice, with a lattice constant b. Thermal bending fluctuations bring neighboring filaments into contact which, in the presence of fascin, can associate and dissociate, resulting eventually in an equilibrium distribution of bundle sizes, N. For simplicity, we assume that all bundles are of the same size, $N = N^*$, corresponding to the value of N, which minimizes the energy of a system of M filaments organized in M/N bundles of size N, Equation (8):

$$\Delta E = (M/N)\Delta E_{\mathrm{Bund}}(N) \tag{8}$$

with $\Delta E_{\mathrm{Bund}}(N)$ denoting the formation energy of a bundle comprising N filaments [Eq. (9)]:

$$\Delta E_{\mathrm{Bund}}(N) = \Delta E_{\mathrm{Fas}}(N) + \Delta E_{\mathrm{Bend}}(N) \tag{9}$$

The fascin–actin binding terms, both within (cohesion) and at the surface of the bundle are included in ΔE_{Fas}. ΔE_{Bend} is the bending penalty of all N filaments comprising the bundle.

Bundles, like dimers, are modeled as composed of a stem and a root, Figure 6, right. In the stem the filaments are tightly packed into hexagonal bundles (supported by the experimental results[48,49]) with well-defined inter-axial distances, d, between the filaments; d is dictated by the cross linking proteins ($d \approx 9$ nm for fascin[50]). For simplicity we assume that bundle sizes increase in discrete steps, adding one (hexagonal) "closed shell" at a time. Thus, the smallest bundle is a single filament ($N = 1$), next in size is a bundle of $N = 7$ filaments, consisting of a central filament surround by the first ($s = 1$) shell of 6 filaments, then comes a bundle containing 12 additional filaments in the second ($s = 2$) shell, etc. With S denoting the outermost shell, the bundle comprises $N = 3\,S(S+1)+1$ filaments, $6\,S = \sqrt{12}N^{1/2}\sqrt{1 - 1/4\,N} - 3 \approx 2\sqrt{3}N^{1/2} - 3$ of which are in the surface layer.

In Figure 6, the stem describing the straight part of the bundle is depicted as a cylinder whose bottom is capped by an inverted cone. Its top surface appears flat. This geometry is, in fact, a very good approximation to the geometry of the stem derived by detailed energetic calculations.[51] The shape of the stem enters the calculation of both the bending and the binding energy of the bundle. Its formation energy can be expressed as a sum of a cohesive (negative energy) term, as if all N filaments were fully surrounded by neighbors, and an unfavorable (positive) surface term accounting for the smaller (about one half) number of neighbors to filaments in the surface layer [Eq. (10)]:

$$\Delta E_{\mathrm{Fas}}(N) = \theta_D \varepsilon_D [\rho V(N) - 0.5\,\sigma A(N)] \tag{10}$$

where $V(N)$ and $A(N)$ are, respectively, the volume and surface area of the stem, as illustrated in Figure 6 (their detailed derivations are outlined elsewhere[51]). $\rho = 1.6 \times 10^6\ \mu\mathrm{m}^{-3}$ and $\rho = 9.3 \times 10^3\ \mu\mathrm{m}^{-2}$ are the volume and surface densities of fascin D-sites: σ and ρ are calculated using previous data,[41,42,48–50] by taking into account the helix structure of actin-fascin bundles,

namely, we assume that filaments in the interior of a bundle have six nearest neighbors and filaments in the surface of the bundle have about half the number of neighbors. Then, knowing the (average) distance between neighboring filaments in a bundle, and the distance between adjacent fascin binding sites along F-actin filaments, the calculation of is straightforward.

The bending energy of the root, $\Delta E_{\mathrm{Bend}}(N)$, is a sum of contributions from the individual filaments. Following similar arguments to those used in Section 2.1, the optimal length of the bent portion of a filament belonging to layer s of the bundle is $l^* = [\chi b^2 \lambda/(\theta_D|\varepsilon_D|)]^{1/4} s^{1/2}$. For deriving l^*, we assume that the cross-linking energy per unit length of a filament is calculated at the bulk of a bundle (for all shells), yielding $3\theta_D\varepsilon_D/\lambda$ (this approximation was done only for the geometrical derivation, and was not needed for calculating ΔE_{Fas}[51]). The bending energy of the filament is thus $\chi b^2 s^2/l^{*3} = \chi^{1/4} b^{1/2} (\theta_D|\varepsilon_D|/\lambda)^{3/4} s^{1/2}$.

Integrating over all shells, we obtain the total bending energy of the bundle as Equation (11):

$$E_{\mathrm{Bend}} = \frac{5\pi\xi}{\alpha^3} s^{5/2} = \left(\frac{5}{\sqrt{3}}\right) \frac{5\pi\xi}{\alpha^3} \left(N^{1/2} - \sqrt{3}/2\right)^{5/2} \qquad (11)$$

The optimal bundle size, N^*, can now be evaluated by substituting Equations (10) and (11) into Equation (9) and then into Equation (8), followed by a minimization of ΔE with respect to N. For the relatively small values of N of interest herein, the minimization needs to be done numerically. Calculated values of N^* are shown in Figure 7 as a function of f, for

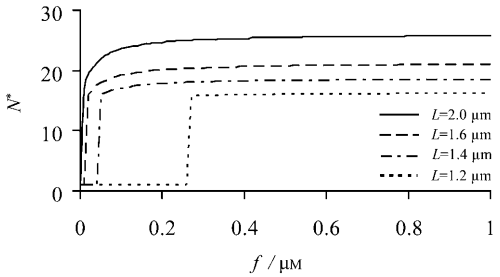

Figure 7. Most probable bundle size as a function of fascin concentration in solution, for $b = 0.2$ μm and several values of L.

$b = 0.2$ μm and several different values of L, ranging from 1.2 to 2 μm. Note the existence of a minimal f for bundle formation, for example, for $L = 1.2$ μm, bundles become stable only for $f \geq 0.27$ μM. The slightly longer filaments of 1.4 μm will form stable bundles already at $f = 0.05$ μM. This behavior reflects the fact that in order for bundle to form, the cohesive energy of the stem must exceed the bending energy of the root. If L is small, the length of the stem is necessarily small and the minimal cohesive energy is only achieved upon increasing the number of cross linkers, that is, by increasing f. As L increases, this requirement is satisfied by lower f. Interestingly, for the two low L values in Figure 7, N jumps discontinuously from 1 to more than 15, suggesting that for this range of L, where the stems are necessarily short, the cohesive energy requires not only an increase in f, but also in the number of cross-linked filaments. (This occurs because the bending energy increases less strongly with N, as compared to the cohesive energy gain.[51])

3. Conclusions

Our primary goal herein was to explore the conditions underlying the transition from a densely branched network of actin filaments into long finger-like bundles of filaments. The general motivation to study this phenomenon is because it is reminiscent of the biologically abundant and important phenomenon of lamellipodium-to-filopodia transition. The specific model system that we chose to analyze is far simpler, and yet it involves three of the most important rate processes in the real system: polymerization, branching and cross-linking. In the in vitro experiments that accompany the present study, these processes are mediated by three proteins—actin, Arp2/3 complex, and fascin. Various other processes and proteins participate in the dynamical behavior of the actin network and its morphological transitions in the living cell, as discussed briefly below. We believe that the basic conclusions derived from our simple model system are of more general significance. For example, a simple relationship between filament length and distance at the onset of bundling [similar to the inequality of Eq. (7)], could possibly unravel some of the complex biological factors that control the formation of filopodia.

Our basic assumption in modeling the aster-to-star transition and the subsequent growth of bundles is that these processes are governed by the interplay between two major energetic factors: bending energy on the one hand, and cross-linker-mediated adhesion on the other. Detailed KMC simulations were performed in order to derive numerical values of L and b, as a function of time, which together with f determine the onset of bundling. However, then, to simplify the mathematical description we have various approximations, for example, that all filaments at the aster periphery are of the same length and are initially normal the supposedly planar surface, and that when they bend they look like complementary arcs. We believe that these are harmless approximations of no qualitative and limited quantitative influence on our conclusions. Considerably more drastic approximations and assumptions entered our formulation of both the irreversible step-wise mechanism, and the reversible equilibrium model for bundle size. These include the assumption of monodisperse size distribution (in both models), the discrete "shell model" of bundle sizes, the use of a hexagonal lattice to describe filament positions, and the approximate evaluations of the corresponding energetic factors. Notwithstanding all these reservations, we reiterate that both models were primarily meant to present different possible qualitative scenarios of bundle maturation. We close this section with a brief discussion of the biological context of our models.

Apart from fascin, various other linkage proteins (e.g. mDia2 and Ena/VASP) play a major role in filament bundling in living cells; some, in addition to their role as cross-linkers of actin,

serve also as anti-cappers, keeping filaments long.[25,33,34] Actually, it has been shown that fascin is mainly involved in bundle growth and maintenance, and probably does not take an active part in the early stages of bundle nucleation.[34] Nevertheless, we believe that the interplay between bending and binding energies underlying our fascin-mediated bundling model is also in the basis of the more complex lamellipodium-to-filopodia transition. Furthermore, the simple physical arguments presented herein may explain why proteins like mDia2 and Ena/VASP that function as anti-cappers are more likely to nucleate bundles than fascin; we showed herein that long filaments bundle more easily because of the bending–binding interplay. Thus tip-complex proteins that keep filaments long and are also able to cross-link them are more likely to serve as cross-linkers than fascin. Indeed, several proteins that control filament length (some tip-complex proteins and other regulators of capping activity) were found to dramatically enhance the formation of filopodia formation.[24,25,33–35]

Below we briefly and qualitatively further examine how several different types of linkage proteins behave at the onset of bundling, regardless of their effect (if any) on filament length. In living cells, bundles are nucleated by the formation of Λ-precursor shapes of actin, assembled by tip-complex proteins.[34] Two possible models of an initial actin assembly, mediated by tip-complex proteins, are proposed in Figure 8, alongside the fascin-mediated structure. One model describes a nucleus involving two actin filaments, while the other is tetrameric (as may be the case when Ena/VASP is the cross-linking protein[52,53]). The three models shown differ in the geometry of the bent filaments. Fascin cross-links the filaments only when they actually touch and run parallel to each other, Model A in Figure 8. Model B is for a more flexible tip-complex cross-linker (which binds only filament tips) that does not strongly restrict the orientation of the joining filaments. Possible examples may be mDia2 or Ena/VASP.[25,33] Finally, Model C depicts a flexible tip complex (e.g. Ena/VASP) that nucleates an actin tetramer. Figure 8d was originally published in Svitkina et al.[34] and shows an EM image of such a tetramer, perhaps involving Ena/VASP at its tip.

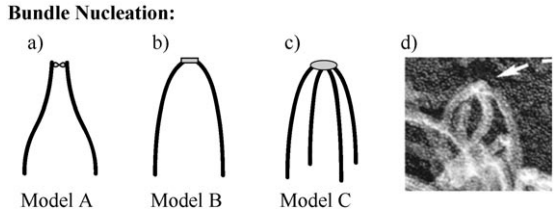

Figure 8. a)–c) Three simple models that describe the geometries of a bundle nucleus. All filaments are of the same length, and the distances between their fixed origins is the same. d) An electron micrograph of a nucleating bundle, forming a tetramer (similar to model C), © Svitkina et al., 2003. Originally published in *J. Cell Biol.* **2003**, *160*, 409–421.[34]

In order to compare the ability of the three structures to stabilize a bundle nucleus, we calculate the bending energies in each of these cases, which the binding energy must overcome. (Unfortunately, no clear data is available regarding the cross-linking energy of many proteins that take place in filopodia formation.) We again assume that all filaments are of length L, with their origins a distance b apart; the bottom ends of the filaments are perpendicular to the surface both before and after bending. For simplicity, the cross-linking is supposed to take place exactly and only at the tip, including in the case of fascin. For model A we already found in Equation (2) that $E^{A}_{bend} = 8\xi kTb^2/L^3$. A simple geometrical calculation shows that the radius of curvature in model B is $R = 2L\sqrt{L^2 - (b/2)^2}/b$, and hence $E^{B}_{bend} = 8\xi kTb^2/[8L(L^2 - (b/2)^2)]$. Finally, for model C $E^{C}_{bend} = 4E^{B}_{bend}\left(L, b\sqrt{2}/2\right) = \xi kTb^2/[4L(L^2 - b^2/8)]$.

From the EM images reported for instance in Svitkina et al.,[34] it appears that the typical length of filaments which nucleate into bundles is $L \sim 0.4$ μm, and the distance between their pointed ends is $b \sim 0.02$ μm. These numbers imply $E^{A}_{bend} = 0.5\,kT$, $E^{B}_{bend} = 0.0087\,kT$ and $E^{C}_{bend} = 0.016\,kT$. Clearly then, if fascin has to nucleate bundling, which requires that the filaments must first get parallel to each other, the concomitant bending energy penalty is much higher than in the other two cases. This notion is an additional support that explains why fascin is not dominant in the early nucleation of filopodia in living cells.

To conclude, the simple physical principle of competition between bending and binding energies appears to adequately explain the transition from an isotropic aster-like network to a star-like structure with bundles emanating from the aster's core. However, similar arguments appear to suggest that fascin does not play a dominant role in the first stages of bundle formation in the lamellipodia-to-filopodia transition. The simple model calculations presented above suggest that other proteins, like mDia2 and Ena/VASP will participate in bundle nucleation in living cells. On the other hand, the large fascin-mediated cross-linking energy, and hence the rigidity and strength of the bundles, support the notion that fascin effectively stabilizes pre-formed bundles, as reported to be the case in living cells.[34]

Experimental Section

Protein Purification: Actin was purified from rabbit skeletal muscle acetone powder.[54] Recombinant WASp-VCA[30] and fascin (recombinant fascin was prepared by a modification of the method presented in Ono et al.[55]) were expressed in *E. coli* as GST fusion proteins. Arp2/3 complex was purchased from Cytoskeleton Co. Actin was labeled on Cys374 with Alexa fluor 568 or 488 (Invitrogen, Co.).

Microscopy: Actin assembly was monitored for about an hour by fluorescence with an Olympus IX-71 microscope. The labeled actin fraction was 1/40 and the temperature was 22 °C. Time-lapse images were acquired using an Andor DV887 EMCCD camera (Andor Co., England). Data acquisition and analysis was performed using METAMORPH (Universal Imaging Co.).

Bundle length: Few tens of bundles were used to determine the mean value of bundles length for each fascin concentration. The bundle length was measured from the visible end of the bundle to the middle of the stars' core (using MetaMorph software). For each fascin concentration we extracted the mean length ± SD.

Acknowledgements

We thank Tatyana M. Svitkina for her biologically insightful comments and Anders S. Carlsson for useful discussions, information and data. We also thank the organizing committee for inviting us to contribute an article to this Festschrift to Professor Sackmann. Y.B.K. thanks the Maydan foundation for her PhD fellowship. A.B.G. thanks the financial support of the Joseph and May Winston Foundation Career Development Chair (Grant No. 20070020B) and the Israel Science Foundation (ISF grant No. 551/04). A.B.S. is grateful for the support of the ISF (Grant No. 659/06), the US–Israel Binational Science Foundation (BSF grant 2006-401), and the Archie and Marjorie Sherman Chair. The Fritz Haber Research Center is supported by the Minerva foundation.

Keywords: filaments · kinetic Monte Carlo · polymerization · proteins · self-assembly

[1] T. D. Pollard, G. G. Borisy, *Cell* **2003**, *112*, 453 – 465.
[2] S. M. Rafelski, J. A. Theriot, *Annu. Rev. Biochem.* **2004**, *73*, 209 – 239.
[3] J. V. Small, T. Stradal, E. Vignal, K. Rottner, *Trends Cell Biol.* **2002**, *12*, 112 – 120.
[4] E. S. Chhabra, H. N. Higgs, *Nat. Cell Biol.* **2007**, *9*, 1110 – 1121.
[5] K. Keren, Z. Pincus, G. M. Allen, E. L. Barnhart, G. Marriott, A. Mogilner, J. A. Theriot, *Nature* **2008**, *453*, 475 – 480.
[6] G. Ladam, L. Vonna, E. Sackmann, *Acta Biomater.* **2005**, *1*, 485 – 497.
[7] A. B. Verkhovsky, T. M. Svitkina, G. G. Borisy, *Curr. Biol.* **1999**, *9*, 11 – 20.
[8] T. M. Svitkina, G. G. Borisy, *J. Cell Biol.* **1999**, *145*, 1009 – 1026.
[9] D. Pantaloni, C. Le Clainche, M. F. Carlier, *Science* **2001**, *292*, 1502 – 1506.
[10] T. D. Pollard, *Nature* **2003**, *422*, 741 – 745.
[11] N. Q. Balaban, U. S. Schwarz, D. Riveline, P. Goichberg, G. Tzur, I. Sabanay, D. Mahalu, S. Safran, A. Bershadsky, L. Addadi, B. Geiger, *Nat. Cell Biol.* **2001**, *3*, 466 – 472.
[12] B. Geiger, J. P. Spatz, A. D. Bershadsky, *Nat. Rev. Mol. Cell Biol.* **2009**, *10*, 21 – 33.
[13] E. Puklin-Faucher, M. P. Sheetz, *J. Cell Sci.* **2009**, *122*, 575 – 575.
[14] B. Wehrle-Haller, B. A. Imhof, *Int. J. Biochem. Cell Biol.* **2003**, *35*, 39 – 50.
[15] J. A. Theriot, T. J. Mitchison, *Nature* **1991**, *352*, 126 – 131.
[16] M. Prass, K. Jacobson, A. Mogilner, M. Radmacher, *J. Cell Biol.* **2006**, *174*, 767 – 772.
[17] J. Faix, D. Breitsprecher, T. E. Stradal, K. Rottner, *Int. J. Biochem. Cell Biol.* **2009**, *41*, 1656 – 1664.
[18] M. F. Olson, E. Sahai, *Clin. Exp. Metastasis* **2009**, *26*, 273 – 287.
[19] H. Zhang, J. S. Berg, Z. Li, Y. Wang, P. Lang, A. D. Sousa, A. Bhaskar, R. E. Cheney, S. Stromblad, *Nat. Cell Biol.* **2004**, *6*, 523 – 531.
[20] T. H. Hsu, M. H. Yen, W. Y. Liao, J. Y. Cheng, C. H. Lee, *Lab Chip* **2009**, *9*, 884 – 890.
[21] Y. Hashimoto, M. Parsons, J. C. Adams, *Mol. Biol. Cell* **2007**, *18*, 4591 – 4602.
[22] L. M. Machesky, *FEBS Lett.* **2008**, *582*, 2102 – 2111.
[23] F. Korobova, T. Svitkina, *Mol. Biol. Cell* **2008**, *19*, 1561 – 1574.
[24] M. R. Mejillano, S. Kojima, D. A. Applewhite, F. B. Gertler, T. M. Svitkina, G. G. Borisy, *Cell* **2004**, *118*, 363 – 373.
[25] C. Yang, L. Czech, S. Gerboth, S. Kojima, G. Scita, T. Svitkina, *PLoS Biol.* **2007**, *5*, e317.
[26] J. Faix, K. Rottner, *Curr. Opin. Cell Biol.* **2006**, *18*, 18 – 25.
[27] A. Steffen, J. Faix, G. P. Resch, J. Linkner, J. Wehland, J. V. Small, K. Rottner, T. E. Stradal, *Mol. Biol. Cell* **2006**, *17*, 2581 – 2591.
[28] L. Haviv, Y. Brill-Karniely, R. Mahaffy, F. Backouche, A. Ben-Shaul, T. D. Pollard, A. Bernheim-Groswasser, *Proc. Natl. Acad. Sci. USA* **2006**, *103*, 4906 – 4911.
[29] Y. Ideses, Y. Brill-Karniely, L. Haviv, A. Ben-Shaul, A. Bernheim-Groswasser, *PLoS One* **2008**, *3*, e3297.
[30] A. Bernheim-Groswasser, S. Wiesner, R. M. Golsteyn, M. F. Carlier, C. Sykes, *Nature* **2002**, *417*, 308 – 311.
[31] T. D. Pollard, L. Blanchoin, K. J. Amann, H. N. Higgs, J. B. Marchand, D. A. Kaiser, *Nature* **2000**, *404*, 1007 – 1011.
[32] P. Kraikivski, B. M. Slepchenko, I. L. Novak, *Phys. Rev. Lett.* **2008**, *101*, 128102.
[33] D. A. Applewhite, M. Barzik, S. Kojima, T. M. Svitkina, F. B. Gertler, G. G. Borisy, *Mol. Biol. Cell* **2007**, *18*, 2579 – 2591.
[34] T. M. Svitkina, E. A. Bulanova, O. Y. Chaga, D. M. Vignjevic, S. Kojima, J. M. Vasiliev, G. G. Borisy, *J. Cell Biol.* **2003**, *160*, 409 – 421.
[35] D. Vignjevic, S. Kojima, Y. Aratyn, O. Danciu, T. Svitkina, G. G. Borisy, *J. Cell Biol.* **2006**, *174*, 863 – 875.
[36] D. Vignjevic, J. Peloquin, G. G. Borisy, *Methods Enzymol.* **2006**, *406*, 727 – 739.
[37] D. Vignjevic, D. Yarar, M. D. Welch, J. Peloquin, T. Svitkina, G. G. Borisy, *J. Cell Biol.* **2003**, *160*, 951 – 962.
[38] H. Isambert, P. Venier, A. C. Maggs, A. Fattoum, R. Kassab, D. Pantaloni, M. F. Carlier, *J. Biol. Chem.* **1995**, *270*, 11437 – 11444.
[39] P. A. Janmey, S. Hvidt, J. Kas, D. Lerche, A. Maggs, E. Sackmann, M. Schliwa, T. P. Stossel, *J. Biol. Chem.* **1994**, *269*, 32503 – 32513.
[40] L. Yang, D. Sept, A. E. Carlsson, *Biophys. J.* **2006**, *90*, 4295 – 4304.
[41] M. F. Schmid, J. M. Agris, J. Jakana, P. Matsudaira, W. Chiu, *J. Cell Biol.* **1994**, *124*, 341 – 350.
[42] N. Volkmann, D. DeRosier, P. Matsudaira, D. Hanein, *J. Cell Biol.* **2001**, *153*, 947 – 956.
[43] I. Borukhov, R. F. Bruinsma, W. M. Gelbart, A. J. Liu, *Proc. Natl. Acad. Sci. USA* **2005**, *102*, 3673 – 3678.
[44] A. E. Carlsson, *Phys. Rev. Lett.* **2004**, *92*, 238102.
[45] M. Bathe, C. Heussinger, M. M. Claessens, A. R. Bausch, E. Frey, *Biophys. J.* **2008**, *94*, 2955 – 2964.
[46] M. M. Claessens, M. Bathe, E. Frey, A. R. Bausch, *Nat. Mater.* **2006**, *5*, 748 – 753.
[47] A. Mogilner, B. Rubinstein, *Biophys. J.* **2005**, *89*, 782 – 795.
[48] L. G. Tilney, P. S. Connelly, K. A. Vranich, M. K. Shaw, G. M. Guild, *J. Cell Biol.* **2000**, *148*, 87 – 100.
[49] L. G. Tilney, M. S. Tilney, G. M. Guild, *J. Cell Biol.* **1995**, *130*, 629 – 638.
[50] R. Ishikawa, T. Sakamoto, T. Ando, S. Higashi-Fujime, K. Kohama, *J. Neurochem.* **2003**, *87*, 676 – 685.
[51] Y. Brill-Karniely, Ph. D. Thesis, in preparation.
[52] S. Hüttelmaier, B. Harbeck, O. Steffens, T. Messerschmidt, S. Illenberger, B. M. Jockusch, *FEBS Lett.* **1999**, *451*, 68 – 74.
[53] M. Krause, E. W. Dent, J. E. Bear, J. J. Loureiro, F. B. Gertler, *Annu. Rev. Cell Dev. Biol.* **2003**, *19*, 541 – 564.
[54] J. A. Spudich, S. Watt, *J. Biol. Chem.* **1971**, *246*, 4866 – 4871.
[55] S. Ono, Y. Yamakita, S. Yamashiro, P. T. Matsudaira, J. R. Gnarra, T. Obinata, F. Matsumura, *J. Biol. Chem.* **1997**, *272*, 2527 – 2533.

Received: August 3, 2009
Published online on October 21, 2009

